RAA 2021 Vol. 21 No. 12, 307(9pp) doi:10.1088/1674-14527/21/12/307

http://www.raa-journal.org *http://iopscience.iop.org/raa*

Research in Astronomy and Astrophysics

Fabrication of large UV transmission blazed gratings for slitless spectral sky survey

Zhi-Wen Chen[1], Mao-Qi Cai[1], Ke-Qiang Qiu[1], Ya-Nan Wang[1], Huo-Yao Chen[1], Zheng-Kun Liu[1], Ying Liu[1], Yi-Lin Hong[1], Hai-Jiao Jiang[2,3] and Zhong-Wen Hu[2,3]

[1] National Synchrotron Radiation Laboratory, University of Science and Technology of China, Hefei 230029, China; *blueleaf@ustc.edu.cn, zhkliu@ustc.edu.cn*

[2] Nanjing Institute of Astronomical Optics & Technology, National Astronomical Observatories, Chinese Academy of Sciences, Nanjing 210042, China

[3] Key Laboratory of Astronomical Optics & Technology, Chinese Academy of Sciences, Nanjing 210042, China

Received 2021 July 30; accepted 2021 September 22

Abstract Slitless spectral sky survey is a critical direction of international astronomical research. Compared with ground-based sky survey, space-based sky survey can achieve full-band observation, and its imaging quality and resolution capability are restricted by the efficiency and size of dispersive elements. Transmission blazed gratings are often used as the dispersive elements in the UV band. Holographic interference lithography produces the photoresist mask of a grating, and the ion beam etching vertically transfers the pattern to the substrate to form the SiO_2 mask of a grating. To reduce the effect of ion beam divergence on the uniformity of the groove shape, the grating mask is etched tilted by the ion beam passing through a narrow slit to obtain a blazed grating with consistent structural parameters. Moreover, two-dimensional scanning of the sample stage enables the etching of large-size samples. A UV transmission blazed grating with a linear density of 333 lines mm^{-1}, a blazing angle of 11.8°, and a dimension of 99.2 mm × 60.0 mm × 6.0 mm was successfully fabricated with an average diffraction efficiency of 66%, a PV diffraction wavefront of 0.169λ (λ=632.8 nm) and low stray light.

Key words: instrumentation: spectrographs — methods: data analysis — techniques: interferometric

1 INTRODUCTION

Relying on the space station's construction, China has started to develop large-scale sky survey observation projects, usually using large-field telescopes to comprehensively observe the sky (Zhan 2011). According to the difference of terminal instruments, observation projects can be divided into multi-color imaging surveys and slitless spectral surveys. The slitless spectral survey obtains information about celestial bodies by placing a spectrometer on the focal plane, and it can determine not only the composition of celestial bodies, but also the physical conditions such as temperature, pressure, density, magnetic field and velocity of motion, which has become a breakthrough in astronomical observation in the 21st century (Zhao 2014).

Compared with ground-based sky surveys, space-based sky surveys overcome atmospheric perturbations and can achieve extremely high angular resolution. For example, the angular resolution of the Hubble Space Telescope (HST) exceeds 0.1 arcsecond (Burbidge 1978). Moreover, space-based sky surveys reduce the influence of atmospheric absorption and scattering, making it possible to observe the whole spectral band. As an essential component of space spectral sky survey, the slitless spectrometer covers 255 nm ∼ 1000 nm (UV to NIR band). Considering the position relationship between the slitless spectrometer and the telescope focal plane, China's space station multi-color photometry and slitless spectral survey project often select transmission grating as the dispersive element, which has a simple structure and high stability. The incident light is diffracted from the back of the grating at a fixed angle, so low alignment accuracy is required. A blazed grating is selected by optimizing the groove structure to meet the need for high diffraction efficiency. The highest resolution capability is realized by expanding the grating size and increasing the number of grating lines (Chen et al. 2019). Three groups of gratings GU (Ultraviolet), GV (Visible) and GI (Near Infrared) operating in different wavelength bands are spliced together at designed angles and inserted into the converging optical path in front of the telescope focus to achieve wide-band spectral observation. GU, GV and GI work in the wavelengths from 255 nm $\sim$ 420 nm, 400 nm $\sim$ 650 nm, and 620 nm $\sim$ 1000 nm, with line densities of 333 lines mm^{-1}, 235 lines mm^{-1}, and 150 lines mm^{-1} respectively, with the largest grating size of 99.2 mm $\times$ 60.0 mm $\times$ 6.0 mm.

For the visible and near-infrared bands, the HST used replica gratings made by HORIBA Jobin-Yvon (HJY), Cotel et al. (2014) made masters by scribing, selected high transmittance transfer glue for replication, and finally obtained transmission gratings in bulk. However, due to the absence of high transmittance transfer glue in the UV band, the replica grating technique cannot produce UV transmission gratings. With the use of holography-ion beam etching, a photoresist grating mask is obtained by holographic interference lithography, and ion beam etching is used for pattern transfer to get a relief grating on the substrate (Zhuang et al. 1981; Xu et al. 2004, 2005). The substrate material is often used fused silica, which has good transmittance and high stability. In addition, the holographic pattern has no ghost lines and low stray light. Liu et al. (2013) of Soochow University proposed the ion beam tilt etching of homogeneous quartz masks to produce blazed gratings, which would overcame the difficulty to control the consistency of the photoresist mask profile. Dong et al. (2016) of the University of Science and Technology of China have fabricated three types of transmission blazed gratings with 360 lines mm^{-1} and a blazing angle of 16.8° as well as 400 lines mm^{-1} and a blazing angle of 35° and 43° by holography-ion beam etching, and the measured diffraction efficiency can reach more than 75% of the theoretical value. However, the effect of the ion beam divergence is not uniform at different locations from the ion source, resulting in variations of the obtained blazed grating groove parameters, which affect the luminous flux of the dispersive element (Rao et al. 1992). The influence of ion beam divergence is more significant when making large-size transmission gratings.

To solve this problem, a method of two-dimensional scanning etching with a narrow slit is proposed to fabricate large transmission gratings. In this paper, a UV transmission blazed grating with 333 lines mm^{-1}, a blazing angle of 11.8°, and a size of 99.2 mm $\times$ 60.0 mm $\times$ 6.0 mm is fabricated according to the design requirements of the slitless spectral sky survey project for the UV band. First, in Section 2, the basic principle of holography-ion beam etching is described, and the relationship between the incident angle of the ion beam and the blazing angle is established. Then, Sections 3 and 4 analyze the effect of ion beam divergence on the blazing angle in conventional one-dimensional scanning and propose an etching with a narrow slit to correct the relationship between the divergent ion beam and the blazing angle to achieve precise control of groove parameters. Meanwhile, the sample stage is scanned in two dimensions to achieve large-size grating fabrication. Finally, the fabricated UV transmission blazed grating is analyzed and discussed in Section 5.

2 PRINCIPLE OF BLAZED GRATING FORMATION

The process of fabricating a blazed grating by holography-ion beam etching is shown in Figure 2. First, a photoresist layer (a) is spin-coated on fused silica (Norrman et al. 2005; Qiu et al. 2007). Next, a photoresist grating mask (b) is obtained by holographic scanning exposure (Ma & Zeng 2015; Lin et al. 2018). A photoresist grating mask with identical thickness and profile requires complicated photoresist coating and holographic exposure. Therefore, ion beam vertical etching is used to transfer photoresist grating masks with poorly controlled profiles to the substrate to form SiO_2 grating masks (c). Finally, the ion beam is tilted to etch the SiO_2 grating mask until it is entirely etched, forming the blazed grating (d).

Theoretically, we can obtain arbitrary blazing angles by varying the incident angle of the ion beam. As shown in Figure 2, the angle between the incident direction and the normal direction is defined as φ. The point where the tilted ion beam reaches the bottom of the groove is defined as point A. Due to the blocking of the SiO_2 grating mask, the left and right sides of point A receive different fluxes of ion beam bombardment, resulting in the formation of a blazing facet. We replace the SiO_2 grating mask profile with line segments, which move in the direction of their respective normals under the ion beam bombardment. At the next moment, the new profile is formed by the connection of points where the line segments intersect each other (Rangel/ow 1983; Smith & Tagg 1986; Jewett et al. 1977). Based on the geometric relationship between the rates of line segment motion, the following equation is established.

$$\frac{V_s(\varphi+\theta_s)}{\sin(\theta_s)} = -\frac{V_s(\varphi)\cos(\alpha+\varphi)}{\sin(\alpha)\cos(\varphi)}\,, \tag{1}$$

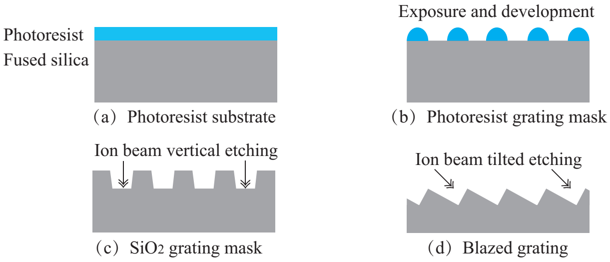

Fig. 1 Process of fabricating blazed gratings.

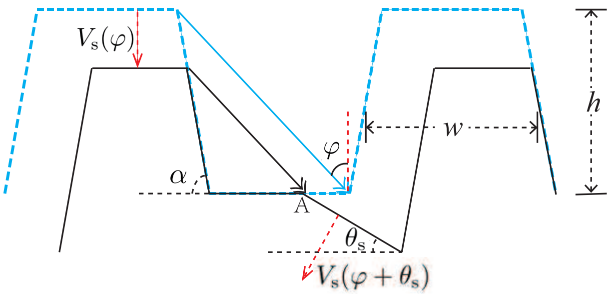

Fig. 2 Geometric relationship between the incident angle of the ion beam and the blazing angle.

where $V_s(\varphi)$, $V_s(\varphi + \theta_s)$ denote the moving rate of the top edge and the blazing facet, θ_s, φ, α denote the blazing angle, the ion beam incident angle, and the inclination angle of the sidewall of the SiO_2 grating mask, respectively, and *h*, *w* denote the height and width of the SiO_2 grating mask.

The SiO_2 grating mask is etched at the incident angle φ of the ion beam. When the height *h* and width *w* shrink to a point simultaneously, the etching of the blazed grating is completed.

3 TRADITIONAL ONE-DIMENSIONAL SCANNING ETCHING

Ion beam etching is often used to transfer the pattern to the substrate. In this paper, we use CHF_3 as the working gas for reactive ion beam etching. The ion beam etching machine uses a 6 cm $\times$ 66 cm Radio Frequency (RF) strip ion source developed by Ion Tech, USA. As shown in Figure 3, the sample to be etched is scanned uniformly along the *x*-direction to achieve a large etching area. The beam diaphragm structure is used to improve the uniformity of the beam flux on this surface (Dong et al. 2007; Qiu et al. 2012).

First, the substrate is placed tilted so that the distance from the surface to the ion source varies linearly in the *y*-direction and the sputtering yield by the ion beam bombarded will also change. Secondly, the ion beam divergence is not completely uniform after leaving the grid

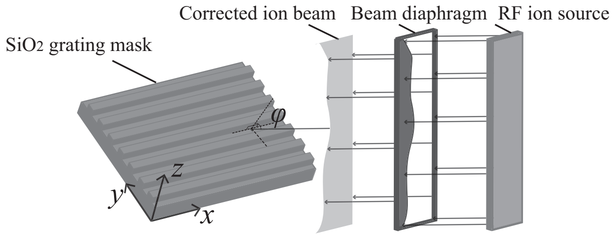

Fig. 3 Diagram of the one-dimensional scanning etching structure.

hole (Ryan et al. 1990; Whealton 1978). The relationship in Equation (1) is based on the premise that the ion beam is perfectly collimated. If considering the divergence of the ion beam, it can be viewed as a Gaussian distribution centered on the incident angle φ in the collimated state, possessing an angular expansion of $2\Delta\varphi$ at 1/2 intensity. The actual etching rate is obtained by weighted averaging of the ion beam etching rate $V_s(\varphi)$ with the Gaussian angle distribution, then finding the incident angle $\varphi_{\rm eff}$ of the effective ion beam that matches it. $\varphi_{\rm eff}$ is used to replace φ in Equation (1) to obtain the blazing angle given the ion beam divergence. Figure 4(a) shows the theoretically calculated relationship between the blazing angle and the ion beam incident angle under different divergence angles ($\Delta\varphi$). With the same ion beam incident angle φ, the smaller the divergence angle is, the smaller the blazing angle is. Therefore, different blazing angles will be formed when etching a large-size grating substrate at a fixed tilt angle due to different divergence. The diffraction efficiencies of the grating under collimated and divergent ion beam etching are simulated by rigorous coupled wave analysis (RCWA) theory, and the diffraction efficiency of the grating etched by divergent ion beam is characterized by the average of the diffraction efficiencies simulated by different blazing angles, and the results are shown in Figure 4(b). The non-uniformity of the blazing angle leads to the decrease of the diffraction efficiency of the grating, which significantly affects the luminous flux of the grating.

4 TWO-DIMENSIONAL SCANNING ETCHING FOR UV TRANSMISSION BLAZED GRATINGS

In the one-dimensional scanning, the distribution of the blazing angle along the *x*-direction is more uniform than the *y*-direction. To ensure that the blazing angle is also uniform in the *y*-direction, a new scanning etching along the *y*-direction is added, while a narrow slit is used to limit the range of the effective ion beam. The smaller the slit width is, the smaller the effect of ion beam divergence is, and accordingly, the slower the etching velocity is. On the basis of a large amount of experimental data, we

Table 1 Ion Beam Etching Parameters and SiO_2 Mask Parameters

Incident angle of ion beam (φ)	Grating period	Mask height (h)	Mask width (w)
65.5°	3003 nm	790 nm	800 nm

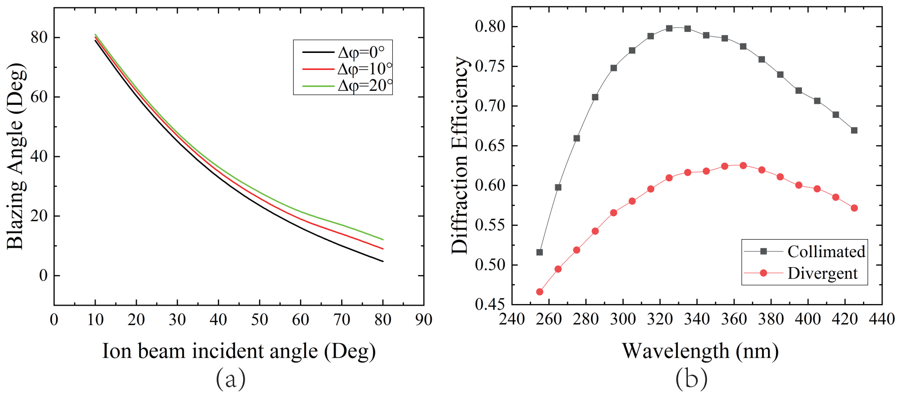

Fig. 4 (a) Influence of the divergence angle of the ion beam on the blazing angle. (b) Effect of the collimated and divergent ion beams on diffraction efficiency.

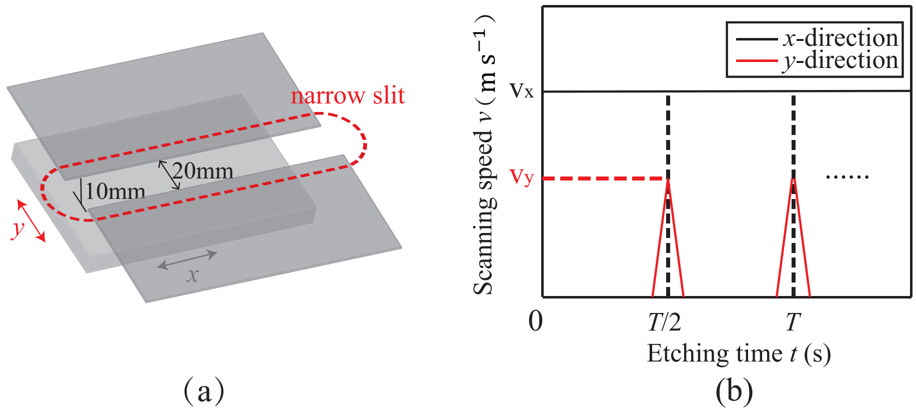

Fig. 5 (a) Schematic of the two-dimensional scanning etching. (b) The motion state of *x*-direction and *y*-direction.

determined the opening size of the slit was 20 mm, and the graphite baffle was placed 10 mm high above the sample, as shown in Figure 5(a). Thus, the *y*-direction takes a step scanning, half a cycle in the *x*-direction, and a step of 20 mm in the *y*-direction, where the step distance is referenced from the slit width, as shown in Figure 5(b), the cycle time T indicates the time spent for one round trip of the workbench.

Based on the analysis of the relationship between the divergent ion beam and the blazing angle in Sections 2 and 3, the optimized ion beam etching parameters and the SiO_2 mask parameters are shown in Table 1, and the groove shape of the fabricated large-size grating was measured using an atomic force microscope (AFM) to analyze the variation of the blazing angle and the anti-blazing angle, and the self-built optical path was used for the spatial distribution of the diffraction efficiency of the fabricated grating.

5 RESULTS AND DISCUSSION

As shown in Figure 6, a UV transmission blazed grating with 333 lines mm^{-1}, a blazing angle of 11.8°, and a size of 99.2 mm × 60.0 mm × 6.0 mm was fabricated by ion beam etching of the tilted sample with a narrow slit two-dimensional scanning. The SEM image and digital camera photo are shown in Figure 7. Compared with the conventional one-dimensional scanning etching, the uniformity of the blazing angle has been dramatically improved, and the overall diffraction efficiency of the grating has been greatly enhanced.

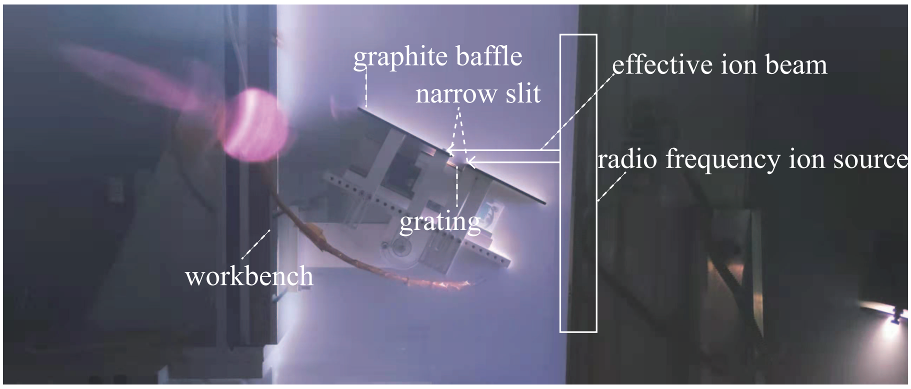

Fig. 6 Internal structure of the two-dimensional scanning etching machine.

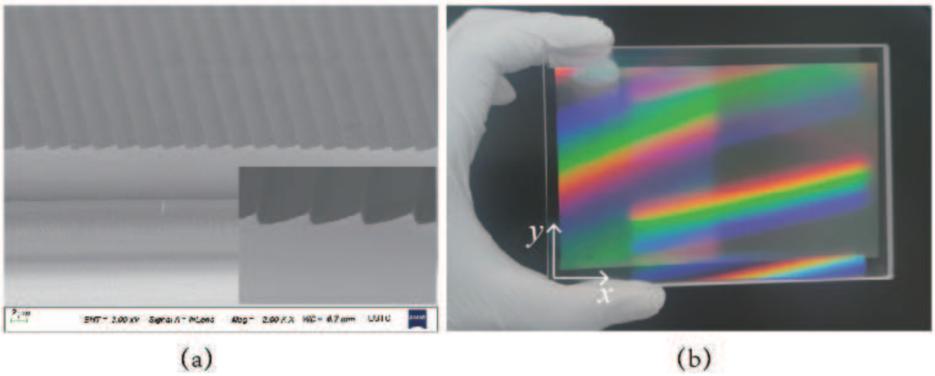

Fig. 7 (a) SEM image of cross section and (b) Digital camera photo of the fabricated GU grating.

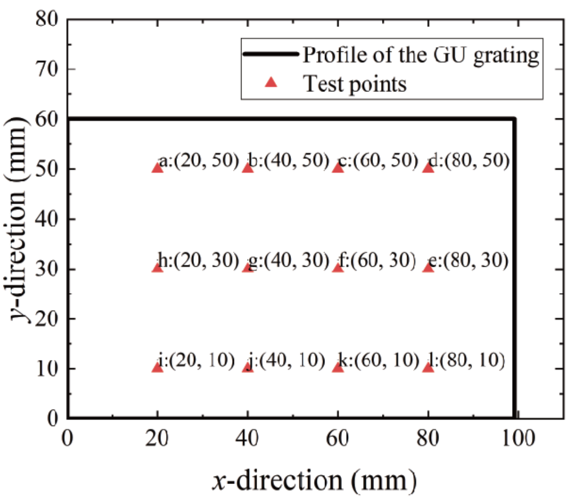

Fig. 8 Spatial distribution of test points.

5.1 Uniformity of Blazing Angle Distribution

To verify the effect of the two-dimensional scanning etching with the narrow slit on the uniformity of the blazing angle distribution, we performed scanning tests on different positions of the grating with AFM. Combining the axes of Figure 3, the positions of the different test points are expressed by the coordinates (x,y) of their projection in the xoy plane, as shown in Figure 8.

(abcd, efgh, ijkl), (ahi, bgj, cfk, del) are the test points in the x and y directions respectively. Figure 9(a) and Figure 9(b) show the angle distributions after one-dimensional scanning etching and two-dimensional scanning etching with the narrow slit, respectively. From the x-direction, the ranges of blazing angles for the one-dimensional scanning are 1.1°, 1.2° and 1.1°, and for the two-dimensional scanning are 1.1°, 0.9° and 1.1°, respectively. This result is consistent with the statements in Sections 3 and 4, where the sample stage is moved in the x-direction, and the effect of the ion beam on the blazing angle is consistent. From the y-direction, the ranges of blazing angles is 3.2°, 3.2°, 3.7° and 3.3° for the one-dimensional scanning and 0.5°, 0.5°, 0.7° and 0.5° for the two-dimensional scanning, respectively. The two-dimensional scanning etching with the narrow slit significantly improves the uniformity of the blazing angles along the y-direction. The average value of the blazing angle for the whole grating surface is 11.825°. Thus, compared with the traditional one-dimensional scanning

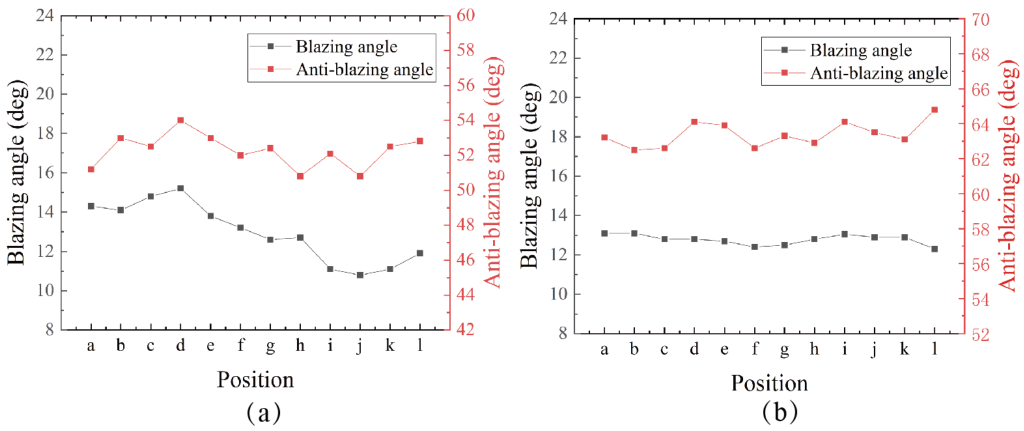

Fig. 9 Angular change of groove shape (a) one-dimensional scanning, (b) two-dimensional scanning.

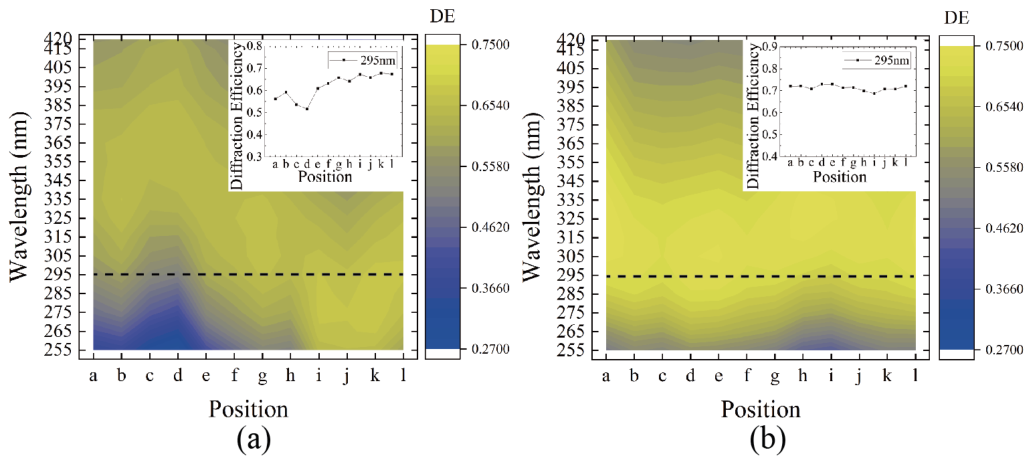

Fig. 10 Diffraction efficiency at different positions (a) One-dimensional scanning, (b) Two-dimensional scanning.

Table 2 Measurements of the Stray Light

	Intensity Ration of the 0th order	Intensity Ration of the +1st order
UV transmission blazed grating	4.05×10^{-3}	3.87×10^{-3}

etching, the two-dimensional scanning etching with the narrow slit can effectively solve the problem of uniformity of the blazing angle for large-size blazed gratings.

5.2 Diffraction Efficiency

5.2.1 Spatial distribution of diffraction efficiency

Using a laser beam in the non-polarized state, the diffraction efficiency of the +1st order at the positions a∼l (positions corresponding to Fig. 8) were tested at an incident angle of 3.8° and wavelengths of 255 nm∼420 nm, and the results are shown in Figure 10, where (a) and (b) are the overall diffraction efficiencies of the samples made by one-dimensional scanning etching and two-dimensional scanning etching with a narrow slit, respectively. As shown in the contour plots, the diffraction efficiency of the samples made by two-dimensional scanning at a certain wavelength does not fluctuate much with position, and the overall diffraction efficiency is more uniform, while the one-dimensional scanning is exactly the opposite. Taking 295 nm as an example, the diffraction efficiency with position distribution of the sample after two-dimensional scanning etching tends to be more linear than one-dimensional scanning etching. The diffraction efficiency with position distribution at the same wavelength is arithmetically averaged to obtain the overall

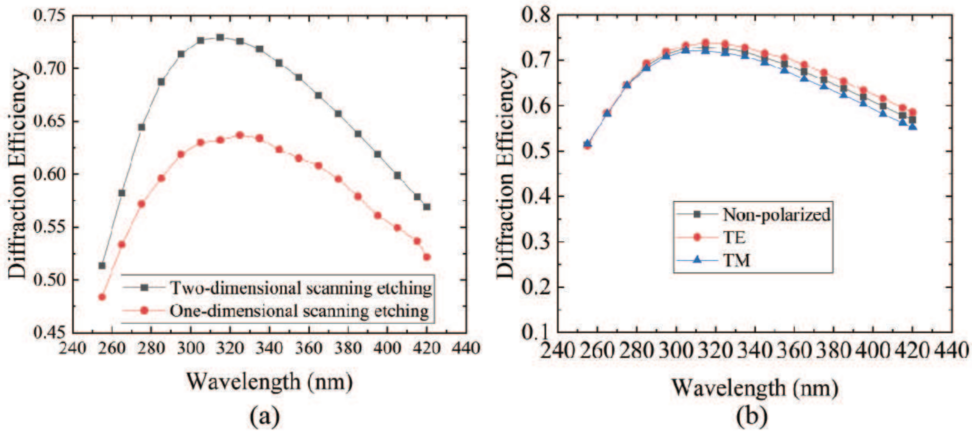

Fig. 11 (a) Diffraction efficiency of the gratings as a function of wavelength for different scanning etching methods. (b) Variation of grating diffraction efficiency under different polarization light.

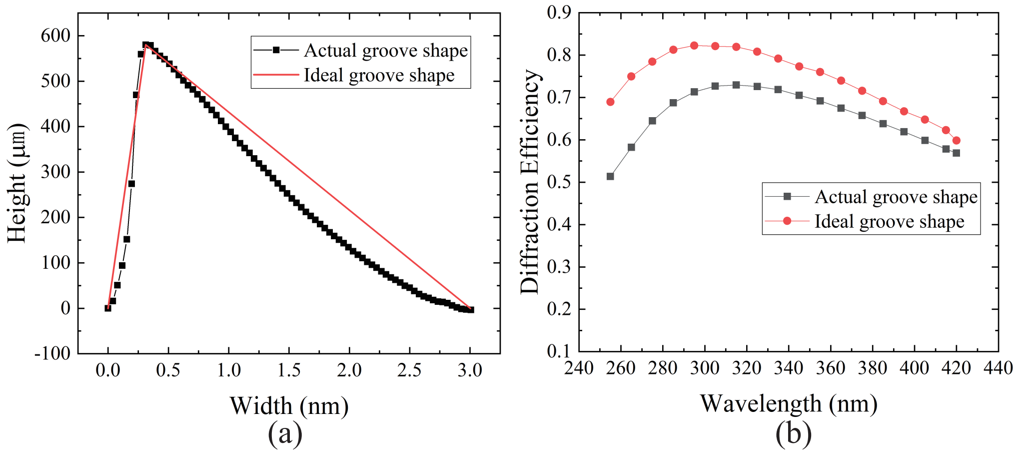

Fig. 12 Effect of (a) deviation of the ideal groove shape from the actual groove shape on (b) diffraction efficiency.

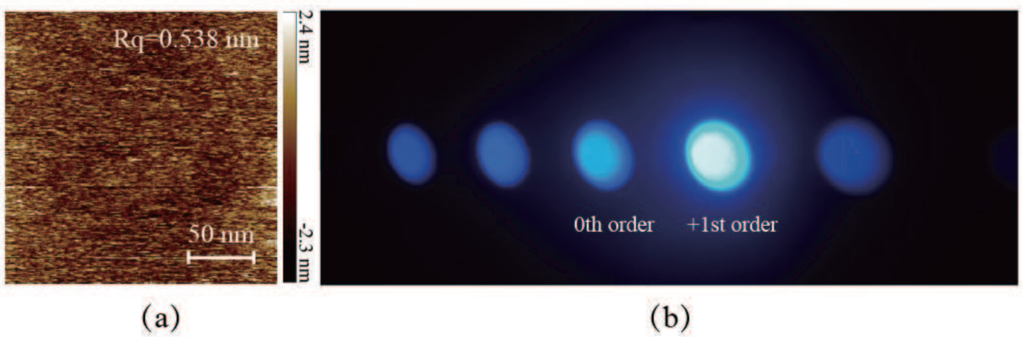

Fig. 13 (a) The roughness of the blazing facet. (b) Diffraction spots at the 0th and +1st orders.

diffraction efficiency of the grating with wavelength, as shown in Figure 11(a), and the trend is the same with Figure 4(b). The two-dimensional scanning etching reduces the influence of the divergent ion beam on the blazing angle and improves the luminous flux of the grating. The average diffraction efficiency can be increased from 52% to 66%. Figure 11(b) shows the variation of diffraction efficiency of UV transmission blazed grating under different polarization light. The TE transmittance is slightly higher than TM near the visible band, but the

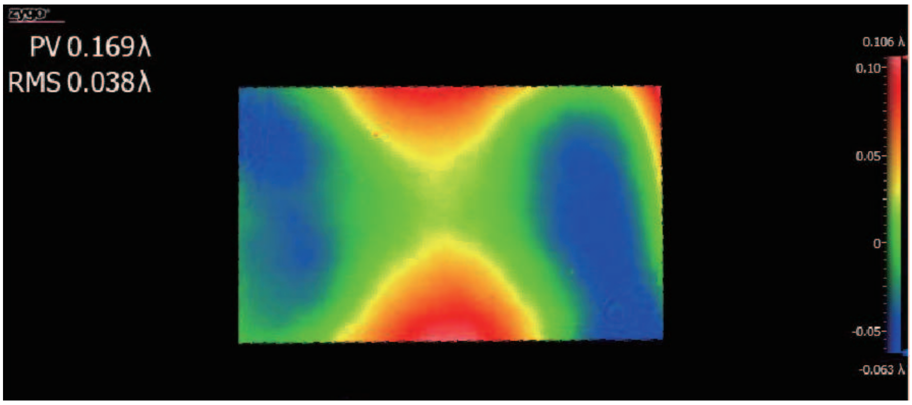

Fig. 14 Results of +1st order diffraction wavefront of UV transmission blazed grating by a Zygo interferometer.

maximum deviation of transmittance at +1st order is not more than 4%. Therefore, UV transmission blazed grating is not sensitive to polarization light and can be applied to any polarization of light passing through.

5.2.2 *Effect of of groove shape on diffraction efficiency*

The actual groove shape of the blazed grating fabricated by holography-ion beam etching is obtained by AFM, and the two terminal points of the bottom are connected with the top point of the groove to form the ideal groove shape, and the difference is shown in Figure 12(a), which shows that there is an internal curve of the blazing facet. Under non-polarized light, the diffraction efficiency obtained from the RCWA simulation of the ideal groove shape is compared with that obtained from the actual groove test, as shown in Figure 12(b). The variation of the diffraction efficiency curve shows that the blazing wavelength position of the actual groove shape shifts towards the long wavelength and the peak diffraction efficiency decreases. The movement of the blazing wavelength position is caused by the curve of the blazing facet. The blue line in Figure 12(a) is the auxiliary line parallel to the blazing facet of the ideal groove, and the blazing angle of the upper left part of the auxiliary line is larger than the blazing angle of the ideal groove, and the upper right part is smaller than the blazing angle of the ideal groove. From the proportion of its distribution, it can be seen that the overall blazing angle is large, resulting in the blazing wavelength position moving to the long wavelength. The decrease in the peak diffraction efficiency is mainly caused by the combination of different blazing angles, as described in Sections 3 and 5.2.1. If there is a need to further improve the diffraction efficiency of the UV transmission blazed grating, this can be achieved by controlling the flatness of the blazing facet.

5.3 Stray Light and Diffraction Wavefront

Holographic scanning exposure averages out high-frequency errors in the interference field by controlling the substrate to scan a shorter distance along the grating line, reducing the grating line curvature and surface roughness of the grating and achieving an improvement in the grating stray light level. Figure 13(a) shows the roughness of the blazing facet with an Rq value of 0.538 nm, and Figure 13(b) shows the spots of 0th and +1st orders by irradiating the UV transmission blazed grating with a 325 nm laser beam, which shows no significant stray light spots around the area.

The stray light test is similar to that of the diffraction efficiency. A laser beam with a wavelength of 325 nm is incident on the grating surface with an incident angle of 3.8°, producing the +1st order of diffraction. We used a small aperture with a diameter close to that of the laser beam to filter out the central spot of the +1st order, and the rest was considered as stray light. The stray light efficiencies around the spots of the +1st and the 0th orders were measured by an integrating sphere, as shown in Table 2. The holography-ion beam etching technique was demonstrated to enable the fabrication of UV transmission blazed gratings with low stray light producing a diffraction at the +1st order.

The diffraction wavefront in the +1st order of the UV transmission blazed grating was detected by a Zygo laser interferometer ($\lambda = 632.8$ nm). Its detection results are shown in Figure 14, with a PV value of 0.169 λ and an RMS of 0.038 λ, which meets the requirement of a PV value of less than 0.5 λ for UV transmission blazed gratings.

6 CONCLUSIONS

This paper presents a method for the fabrication of large-size blazed gratings by two-dimensional scanning etching with a narrow slit. Firstly, the basic principle of holography-ion-beam etching technique for making blazed gratings is introduced. The effect of the inherent divergent nature of the ion beam on the uniformity of the blazing angle in the conventional one-dimensional scanning etching is analyzed. The non-uniformity of the blazing angle directly leads to the degradation of the overall diffraction efficiency of large-size blazed gratings, which affects the imaging quality of slitless spectrometers. The improved process, which controls the divergence angle of the effective ion beam by reserving slits and adds a step scan parallel to the tilt direction, can theoretically realize the fabrication of any large-size blazed grating. Comparisons of the overall blazing angle and diffraction efficiency distribution between the one-dimensional and two-dimensional scanning confirm the effectiveness of the method. A low-stray-light UV transmission blazed grating with a linear density of 333 lines mm^{-1}, a blazing angle of 11.8°, and a size of $99.2\,\mathrm{mm}\times60.0\,\mathrm{mm}\times6.0\,\mathrm{mm}$ was successfully fabricated, with an average diffraction efficiency of 66%, a diffraction wavefront PV of 0.169 λ, for using in a large-scale slitless spectral sky survey project in China.

Acknowledgements This work was supported by the National Natural Science Foundation of China (U1731116). We thank Li Xianghua for proofreading the manuscript. The authors would like to thank the reviewers for their valuable comments to improve the manuscript.

References

Burbidge, E. M. 1978, Phys. Scr, 17, 321
Chen, L. S., Hu, Z. W., & Jiang, H. J. 2019, Acta Astronomica Sinica, 60, 13
Cotel, A., Liard, A., Desserouer, F., Bonnemason, F., & Pichon, P. 2014, in Society of Photo-Optical Instrumentation Engineers (SPIE) Conference Series, 9192, Current Developments in Lens Design and Optical Engineering XV, eds. R. B. Johnson, V. N. Mahajan, & S. Thibault, 91920I
Dong, S. W., Qiu, K. Q., & Fu, S. J. 2016, Vacuum, 53, 54
Dong, X., Liu, Y., Zhao, F., et al. 2007, Journal of University of Science and Technology of China, 37, 530
Jewett, R. E., Hagouel, P. I., Neureuther, A. R., & Van Duzer, T. 1977, Polymer Engineering & Science, 17, 381
Lin, D., Chen, H., Liu, Z., et al. 2018, Optics Letters, 43, 811
Liu, Q., Wu, J., & Chen, M. 2013, Optical Engineering, 52, 091706
Ma, D., & Zeng, L. 2015, Optics Letters, 40, 1346
Norrman, K., Ghanbari-Siahkali, A., & Larsen, N. B. 2005, Annu. Rep. Prog. Chem., Sect. C: Phys. Chem., 101, 174
Qiu, K. Q., Xu, X. D., Hong, Y. L., Liu, Y., & Fu, S. J. 2007, Microfabrication Technology, 19
Qiu, K. Q., Zhou, X. W., Liu, Y., et al. 2012, Optics and Precision Engineering, 20, 1676
Rangel/ow, I. W. 1983, Journal of Vacuum Science Technology A: Vacuum Surfaces and Films, 1, 410
Rao, Y. S., Tang, D. Y., Liu, X. Z., & Shen, B. L. 1992, Journal of Xi'an Jiaotong University, 26, 21
Ryan, T., Chamberlain, P., Brown, I., & Celliers, J. 1990, Journal of Vacuum Science Technology A: Vacuum Surfaces and Films, 8, 3284
Smith, R., & Tagg, M. A. 1986, Vacuum, 36, 285
Whealton, J. H. 1978, Applied Physics Letters, 32, 353
Xu, X. D., Hong, Y. L., Fu, S. J., & Wang, Z. S. 2004, Physics, 33, 340
Xu, X., Hong, Y., & Fu, S. 2005, in Society of Photo-Optical Instrumentation Engineers (SPIE) Conference Series, 5636, Holography, Diffractive Optics, and Applications II, eds. Y. Sheng, D. Hsu, C. Yu, & B. Lee, 165
Zhan, H. 2011, Scientia Sinica Physica, Mechanica & Astronomica, 41, 1441
Zhao, Y. H. 2014, Scientia Sinica Physica, Mechanica & Astronomica, 44, 1041
Zhuang, Y., Liu, G. Q., & Li, Y. G. 1981, Optics and Precision Engineering, 33, 32